

Extraction of spin-averaged rovibrational transition frequencies in HD^+ for the determination of fundamental constants

Jean-Philippe Karr^{a,b} and Jeroen C. J. Koelemeij^c

^aLaboratoire Kastler Brossel, Sorbonne Université, CNRS, ENS-Université PSL, Collège de France, 4 place Jussieu, F-75005 Paris, France; ^bUniversité d'Evry-Val d'Essonne, Université Paris-Saclay, Boulevard François Mitterrand, F-91000 Evry, France; ^cLaserLaB, Department of Physics and Astronomy, Vrije Universiteit Amsterdam, De Boelelaan 1081, 1081 HV Amsterdam, The Netherlands.

ARTICLE HISTORY

Compiled March 28, 2023

ABSTRACT

We present a comprehensive analysis of all currently available high-accuracy frequency measurements of rotational and rovibrational transitions in the hydrogen molecular ion HD^+ . Our analysis utilises the theoretically calculated hyperfine structure to extract the values of three spin-averaged transition frequencies through a global linear least-squares adjustment that takes into account theory-induced correlations between the different transitions. We subsequently use the three spin-averaged transition frequencies as input data in a second adjustment which employs precise theoretical expressions for the transition frequencies, written as a function of the proton, deuteron and electron relative atomic masses, the Rydberg constant, and the proton and deuteron charge radii. Our analysis shows that the HD^+ data may significantly improve the value of the electron relative atomic mass and the proton-electron mass ratio, in particular if combined with recent high-precision measurements of particle atomic masses and mass ratios obtained from Penning traps.

KEYWORDS

Deuterated hydrogen molecular ion; precision rotational-vibrational spectroscopy; ab initio molecular theory; molecular hyperfine structure; fundamental physical constants

1. Introduction

Theoretical predictions of physical quantities are generally based on functional expressions that are derived from theoretical models such as quantum electrodynamics (QED). These expressions are parametrised in terms of fundamental physical constants, such as the electron relative atomic mass and the Rydberg constant. The fundamental constants themselves are determined from precision measurements, often performed on single particles or simple atomic quantum systems, by adjusting their values such that theoretical predictions match the experimental observations as closely as possible. Such adjustments, implemented via least-squares optimization of the constants of interest with respect to large bodies of input data, are carried out by

CONTACT J.-Ph. Karr. Email: karr@lkb.upmc.fr

CONTACT J. C. J. Koelemeij. Email: j.c.j.koelemeij@vu.nl

standards organizations such as the Committee on Data for Science and Technology (CODATA) and the Atomic Mass Data Center (AMDC).

For example, the most precise determinations of the Rydberg constant, R_∞ , and the electric charge radii of the proton, r_p , and the deuteron, r_d , have been obtained from laser spectroscopy of both electronic and muonic hydrogen and deuterium, complemented by high-precision QED theoretical predictions (see Ref. [1] and references therein). By contrast, the relative atomic masses of particles like the electron and light nuclei such as the proton and deuteron have traditionally been determined using Penning-trap experiments and (for the electron) theoretical calculations of bound-state g -factors; for recent examples see Refs. [2–7]. It was recognised already in 1976 by Wing et al. that vibrational spectroscopy of the hydrogen molecular ions, such as H_2^+ and HD^+ , could be used for alternative determinations of particle mass ratios provided that both the measurements and the theory of these three-body, two-center quantum systems would be sufficiently accurate [8]. This concept was extended to laser spectroscopy of antiprotonic helium, $\bar{\text{p}}\text{He}$, by Hori et al. who combined their results with precise ab initio theory for a meaningful determination of the antiproton-electron mass ratio which under the assumption of charge, parity and time reversal (CPT) invariance is equivalent to the proton-electron mass ratio, m_p/m_e [9–11]. As a result, $\bar{\text{p}}\text{He}$ data were included in the 2006 and 2010 CODATA adjustments where they contributed primarily to the value of the electron relative atomic mass, $A_r(e)$ [12, 13]. However, the 2014 and 2018 CODATA adjustments no longer considered $\bar{\text{p}}\text{He}$ after $A_r(e)$ was determined using Penning-trap measurements and QED theory with over one order of magnitude smaller uncertainty [2].

In the last two decades, intensive efforts have been devoted to laser spectroscopy of HD^+ stored in radiofrequency (rf) ion traps. Pioneering experiments demonstrated trapping and sympathetic cooling of HD^+ through co-trapped, laser-cooled beryllium ions [14], and subsequent spectroscopy [15, 16]. Similar approaches were implemented by other research groups [17, 18], leading to various demonstrations of spectroscopy at around the part-per-billion level [16, 19, 20], and determinations of the proton-electron mass ratio at a similar level of precision [20–22]. In recent years the accuracy of rotational and vibrational spectroscopy of HD^+ was improved by nearly three orders of magnitude by use of techniques for Doppler-free excitation [23–25]. Meanwhile also the precision of theoretical (QED) predictions of relevant transition frequencies in HD^+ was strongly improved to below the level of 10 parts per trillion (ppt), such that the uncertainty of theoretically predicted frequencies is now limited by (primarily) the uncertainty of the 2018 CODATA value of m_p/m_e [26–28]. As anticipated by Wing et al. [8] and more recently also by Karr et al. [29], the availability of theoretical and experimental transition frequencies with uncertainties in the low-ppt range enabled a determination of m_p/m_e with a precision of about 20 ppt [23–25]. These values represented not only the most precise determinations of m_p/m_e to date, but they also were found to be consistent with a precise measurement of the proton relative atomic mass, $A_r(p)$, that deviated significantly from other determinations of $A_r(p)$ that were included in the 2018 CODATA adjustment [1, 3, 4]. Furthermore it has been pointed out by several authors that results from HD^+ and $\bar{\text{p}}\text{He}$ are of interest as they form a linking pin between ‘atomic’ fundamental constants such as R_∞ , r_p and r_d , and particle masses and mass ratios that are typically determined using Penning traps, while enabling cross checks of QED calculations of bound-state g -factors of the electron which are relevant to the determination of $A_r(e)$ [30, 31].

The recent advances in HD^+ experiments and theory and their demonstrated potential for the determination of fundamental constants warrant a closer investigation

of the further analysis required to prepare available HD^+ data for a possible inclusion in future CODATA adjustments. One crucial issue here is that, in general, atomic and molecular spectroscopic data include line shifts due to hyperfine interactions, whereas CODATA adjustments have historically considered only energy differences between hyperfine centroids. This implies that experimental spectroscopic data must undergo a preparatory analysis in order to effectively remove the hyperfine shifts from the data. This also applies to the case of HD^+ , and several methods have been developed to derive spin-averaged transition frequencies (i.e. the energy differences between the upper- and lower-state hyperfine centroids) from experimentally measured frequencies of groups of hyperfine components [23, 32]. Here it should be noted that in the absence of independent experimental data on the relevant HD^+ hyperfine structure, the theoretically predicted hyperfine structure is used. In this work we adopt the approach of [32], which is based on a least-squares optimization and takes into account the effect of correlations between theoretical hyperfine coefficients.

This article is organised as follows. The state-of-the-art HD^+ hyperfine theory used for the extraction of spin-averaged transition frequencies is reviewed in Section 2, along with a discussion of correlated hyperfine theory errors. Section 3 summarises the available experimental data (that include hyperfine shifts) related to three different rotational-vibrational transitions in HD^+ , followed by a global adjustment of the three spin-averaged rotational-vibrational transition frequencies in Section 4. In Section 5, the adjusted spin-averaged frequencies and their covariances are subsequently combined with theoretical expressions that are functional expressions of several fundamental constants of interest, including $A_r(e)$, $A_r(p)$, and the deuteron relative atomic mass, $A_r(d)$, thus forming a set of HD^+ observational equations. We use these in a second adjustment, aimed at determining the values of the fundamental constants involved. We consider various sets of input data and observational equations (including e.g. also recent Penning-trap measurements in addition to the HD^+ data), and compare values of mass ratios such as m_p/m_e that are derived from each adjustment, in order to illustrate the potential impact of HD^+ on the precision of fundamental particle mass ratios. Conclusions are presented in Section 6.

2. Status of hyperfine structure theory

2.1. Hyperfine Hamiltonian

The hyperfine structure of a given rovibrational state of HD^+ can be described by the following effective spin Hamiltonian [33]:

$$\begin{aligned}
H_{\text{eff}} = & E_1(\mathbf{L} \cdot \mathbf{s}_e) + E_2(\mathbf{L} \cdot \mathbf{I}_p) + E_3(\mathbf{L} \cdot \mathbf{I}_d) + E_4(\mathbf{I}_p \cdot \mathbf{s}_e) \\
& + E_5(\mathbf{I}_d \cdot \mathbf{s}_e) + E_6\{2\mathbf{L}^2(\mathbf{I}_p \cdot \mathbf{s}_e) - 3[(\mathbf{L} \cdot \mathbf{I}_p)(\mathbf{L} \cdot \mathbf{s}_e) \\
& + (\mathbf{L} \cdot \mathbf{s}_e)(\mathbf{L} \cdot \mathbf{I}_p)]\} + E_7\{2\mathbf{L}^2(\mathbf{I}_d \cdot \mathbf{s}_e) \\
& - 3[(\mathbf{L} \cdot \mathbf{I}_d)(\mathbf{L} \cdot \mathbf{s}_e) + (\mathbf{L} \cdot \mathbf{s}_e)(\mathbf{L} \cdot \mathbf{I}_d)]\} \\
& + E_8\{2\mathbf{L}^2(\mathbf{I}_p \cdot \mathbf{I}_d) - 3[(\mathbf{L} \cdot \mathbf{I}_p)(\mathbf{L} \cdot \mathbf{I}_d) + (\mathbf{L} \cdot \mathbf{I}_p)(\mathbf{L} \cdot \mathbf{I}_d)]\} \\
& + E_9\{\mathbf{L}^2\mathbf{I}_d^2 - \frac{3}{2}(\mathbf{L} \cdot \mathbf{I}_d) - 3(\mathbf{L} \cdot \mathbf{I}_d)^2\},
\end{aligned} \tag{1}$$

where \mathbf{I}_d , \mathbf{I}_p , and \mathbf{s}_e are the spins of the deuteron, proton, and electron, and \mathbf{L} the total angular momentum excluding electron and nuclear spins (denoted by \mathbf{N} in standard

spectroscopic notation). Here and throughout the paper, spin and angular momentum operators are written in units of \hbar and are thus dimensionless. The coefficients E_k , $k = 1, 2, \dots, 9$ depend on the rovibrational state (v, L) . This Hamiltonian includes all the spin-dependent interactions that appear at the leading order ($m\alpha^4$), i.e. in the Breit-Pauli Hamiltonian, except for the proton-deuteron spin-spin contact interaction, which is negligibly small because of the strong Coulomb repulsion.

Additional spin-dependent interactions appear at higher orders ($m\alpha^6$ and above). The largest missing term in Equation (1) is a coupling between proton and deuteron ($\mathbf{I}_p \mathbf{I}_d$) mediated by the electron. The coupling coefficient of this interaction was shown to be on the order of 100 Hz [34], which is much smaller than the theoretical uncertainty of E_4 (see below). The above effective Hamiltonian may thus be considered as complete for our present purposes.

The largest terms in Equation (1) are the electron-proton ($E_4 \sim 900$ MHz in the vibrational ground state) and electron-deuteron ($E_5 \sim 140$ MHz) spin-spin contact interactions. They were calculated with relative uncertainties below 1 ppm [35]. A key element allowing to reach this high accuracy is that the total nuclear correction to E_4 (E_5) was determined from the difference between the experimental ground-state hyperfine splitting of the hydrogen (deuterium) atom and the corresponding nonrecoil, point-particle QED prediction, under the assumption that the nuclear correction is entirely described by a contact (delta-function) term. Uncertainties associated with nuclear corrections are thus suppressed, and the theoretical precision is limited by yet unevaluated higher-order QED terms: (i) nonrecoil corrections, dominated by the contribution of relative order $\alpha(Z\alpha^2) \ln(Z\alpha)$ [36, 37], and (ii) recoil corrections that deviate from the contact-term approximation, i.e. mainly the contribution of relative order $(Z\alpha)^2(m/M)$ [38].

The next largest terms are the spin-orbit ($E_1 \sim 30$ MHz in the vibrational ground state) and spin-spin tensor interactions ($E_6 \sim 8$ MHz, $E_7 \sim 1$ MHz for $L = 1$). They were computed with few-ppm uncertainties through calculation of higher-order corrections at orders $m\alpha^6$ [39] and $m\alpha^7 \ln(\alpha)$ [40, 41]. The uncertainty is dominated by yet unevaluated nonlogarithmic corrections at the $m\alpha^7$ order.

The remaining hyperfine coefficients are much smaller, ranging from $E_8 \sim 3$ kHz to $E_2 \sim 30$ kHz. They were calculated in the framework of the Breit-Pauli Hamiltonian with account of the electron's anomalous magnetic moment [33]. In general, the expected relative accuracy of this approximation is on the order of α^2 , but in this case some second-order contributions induced by the leading hyperfine interaction terms can give larger contributions. Due to this, the relative uncertainty of E_2 , E_3 , and E_8 is estimated to $5\alpha^2$ [41]. In the case of the E_9 term that describes the effect of the deuteron quadrupole moment, second-order terms are too small to significantly influence the uncertainty. The relative uncertainty of E_9 is estimated to 98 ppm [41], which accounts for both the theoretical uncertainty and the uncertainty of the deuteron quadrupole moment value from [42].

State-of-the art values of all the hyperfine coefficients, for ro-vibrational levels involved in published high-precision measurements, are given in Table 1.

In the analysis of HD^+ experimental data, it is important to properly estimate correlations between theoretical errors $\delta E_k(v, L)$ on these coefficients. As shown in [32], the assumed level of correlation can significantly influence the determination of spin-averaged frequencies of rovibrational transitions from an incomplete set of measurements of their hyperfine components. Here, we make assumptions similar to those presented in the Appendix C of [41] (see that reference for details):

- Perfect correlations are assumed between $\delta E_4(v, L)$ and $\delta E_4(v', L')$, as well as between $\delta E_5(v, L)$ and $\delta E_5(v', L')$.
- For the other hyperfine coefficients ($k \neq 4, 5$), correlation coefficients between $\delta E_k(v, L)$ and $\delta E_k(v', L')$ are expected to be positive, but are difficult to estimate. In our analysis, we thus vary these coefficients between 0 and 1 to investigate their influence on the spin-averaged frequencies, and quantify the mean shift and additional uncertainty associated with these correlations.
- Perfect correlations are assumed between $\delta E_2(v, L)$ and $\delta E_3(v, L)$, as well as between $\delta E_6(v, L)$ and $\delta E_7(v, L)$. This stems from the fact the the uncalculated QED terms causing theoretical uncertainties in both coefficients are of the same nature.
- The correlation coefficient between $\delta E_4(v, L)$ and $\delta E_5(v, L)$ is estimated to be $r(E_4, E_5) = 0.4016$.
- No other correlations are assumed between $\delta E_k(v, L)$ and $\delta E_l(v, L)$.
- No correlations are assumed between $\delta E_k(v, L)$ and $\delta E_l(v', L')$ with $k \neq l$ and $(v, L) \neq (v', L')$, except for those that are implied by the above hypotheses, e.g.: $r(E_4(v, L), E_5(v', L')) = r(E_4, E_5) = 0.4016$.

Except for the unknown correlation between $\delta E_k(v, L)$ and $\delta E_k(v', L')$ ($k \neq 4, 5$), we do not consider the effect of uncertainties in other correlation coefficients. Indeed, although these uncertainties are not strictly zero, they are estimated to be too small to have any significant impact on the spin-averaged frequencies.

(v, L)	E_1	E_2	E_3	E_4	E_5	E_6	E_7	E_8	E_9
(0, 0)				925 394.159(860)	142 287.556(84)				
(0, 1)	31 985.417(116)	−31.345(8)	−4.809(1)	924 567.718(859)	142 160.670(84)	8611.299(18)	1321.796(3)	−3.057(1)	5.660(1)
(1, 1)	30 280.736(109)	−30.463(8)	−4.664(1)	903 366.501(839)	138 910.266(82)	8136.858(17)	1248.963(3)	−2.945(1)	5.653(1)
(0, 3)	31 628.097(114)	−30.832(8)	−4.733(1)	920 479.981(855)	141 533.075(83)	948.542(2)	145.597	−0.335	0.613
(9, 3)	18 270.853(62)	−21.304(6)	−3.225(1)	775 706.122(721)	119 431.933(73)	538.999(1)	82.726	−0.219	0.501

Table 1. Theoretical hyperfine coefficients of rovibrational states of HD^+ involved in high-precision measurements, in kHz. Missing numbers in the first line imply a zero value. The values of E_4 , E_5 (E_1 , E_6 , E_7) were calculated in Ref. [35] (Ref. [41]). Those of E_2 , E_3 , E_8 , E_9 are taken from [33]. The value of E_9 has been updated using the latest determination of the deuteron’s quadrupole moment [42].

2.2. Hyperfine splitting

The hyperfine structure of a rovibrational state (v, L) is obtained by diagonalizing the effective spin Hamiltonian (1). The adopted coupling scheme of angular momenta is [33]

$$\mathbf{F} = \mathbf{I}_p + \mathbf{s}_e, \quad \mathbf{S} = \mathbf{F} + \mathbf{I}_d, \quad \mathbf{J} = \mathbf{L} + \mathbf{S}. \quad (2)$$

The matrix elements of the effective spin Hamiltonian in the basis of coupled states $|vLFSJ\rangle$ are calculated using standard angular algebra procedures. J is an exact quantum number, whereas F and S are only approximate quantum numbers. A spin eigenstate is denoted by $|vL\tilde{F}\tilde{S}J\rangle$, which is the state having the largest weight in its decomposition over the coupled basis states. In the following, we omit the $\tilde{}$ symbols for simplicity.

Since the matrix of H_{eff} is block diagonal with blocks of size 4×4 at most, its eigenvalues $E_{\text{hfs}}(v, L, F, S, J)$ can be expressed analytically as a function of the hyperfine interaction coefficients E_k (here it should be noted that the spin coefficients E_k are expressed in frequency units, whereas other energies, such as E_{hfs} , are in energy units).

These expressions are then linearised around the theoretical values of the coefficients using the sensitivity coefficients

$$\gamma_k(v, L, F, S, J) = \frac{1}{h} \frac{\partial E_{\text{hfs}}(v, L, F, S, J)}{\partial E_k}. \quad (3)$$

The theoretical hyperfine shifts E_{hfs} and sensitivity coefficients γ_k of all the levels involved in the measurements to be analysed, are given in Table 2.

(v, L)	(F, S, J)	E_{hfs}/h (kHz)	γ_1	γ_2	γ_3	γ_4	γ_5	γ_6	γ_7	γ_8	γ_9
(0, 0)	(0, 1, 1)	-705 735.655(639)				-0.7367	-0.1688				
	(1, 0, 0)	89 060.984(197)				0.2500	-1.0000				
	(1, 1, 1)	171 894.797(194)				0.2367	-0.3312				
	(1, 2, 2)	302 492.318(235)				0.2500	0.5000				
(0, 1)	(0, 1, 2)	-707 870.694(637)	-0.1070	0.1110	0.9953	-0.7338	-0.1845	0.0100	0.1434	-0.1572	-0.4930
	(1, 0, 1)	79 986.308(204)	-0.4286	-0.3861	0.6539	0.2494	-0.9084	-1.0279	0.8343	0.7206	-0.5019
	(1, 1, 2)	183 682.795(196)	0.3319	0.1539	0.5142	0.2341	-0.3152	0.2555	-0.5821	-0.4019	0.2287
	(1, 2, 1)	269 283.177(241)	-0.5693	-0.5592	-1.7183	0.2500	0.4251	0.0392	-3.3471	-3.2839	-2.9444
	(1, 2, 3)	312 567.273(242)	0.5000	0.5000	1.0000	0.2500	0.5000	-0.5000	-1.0000	-1.0000	-0.5000
	(1, 2, 2)	314 228.466(238)	-0.2249	-0.2649	-0.5096	0.2497	0.4997	1.7345	3.4387	3.5591	1.7643
(1, 1)	(1, 2, 1)	263 806.300(235)	-0.5753	-0.5654	-1.7152	0.2500	0.4296	-0.0105	-3.3687	-3.3063	-2.9087
	(1, 2, 3)	305 099.957(236)	0.5000	0.5000	1.0000	0.2500	0.5000	-0.5000	-1.0000	-1.0000	-0.5000
(0, 3)	(0, 1, 4)	-711 832.144(631)	-0.4142	0.4242	2.9867	-0.7267	-0.2156	0.2750	3.0796	-3.3289	-7.4000
	(1, 2, 5)	338 970.635(290)	1.5000	1.5000	3.0000	0.2500	0.5000	-7.5000	-15.0000	-15.0000	-7.5000
(9, 3)	(0, 1, 4)	-596 833.613(533)	-0.3590	0.3727	2.9847	-0.7303	-0.2017	0.1934	2.4743	-2.7221	-7.3853
	(1, 2, 5)	275 723.281(219)	1.5000	1.5000	3.0000	0.2500	0.5000	-7.5000	-15.0000	-15.0000	-7.5000

Table 2. Theoretical hyperfine shifts (column 3) and sensitivity coefficients (columns 4-12) for all the levels involved in high-precision measurements. Missing numbers for the $(v, L) = (0, 0)$ state imply a zero value. The uncertainties of the hyperfine shifts are calculated assuming no correlation between $\delta E_k(v, L)$ and $\delta E_k(v', L')$ for $k \neq 4, 5$, which provides an upper bound of the uncertainty.

3. Available experimental data

At the time of writing, ppt-range frequency measurements of three rotational-vibrational transitions in HD^+ had been reported in peer-reviewed publications. These are the $(v, L): (0, 0) \rightarrow (0, 1)$ rotational transition at 1.31 THz [23], the $(v, L): (0, 0) \rightarrow (1, 1)$ rovibrational transition at 58.6 THz [25], and the $(v, L): (0, 3) \rightarrow (9, 3)$ vibrational overtone at 415 THz [24]. All frequency measurements were made on HD^+ ions stored in an rf trap, and sympathetically cooled to millikelvin temperatures via laser-cooled Be^+ ions stored in the same trap. For further details on the experimental setups and the justification of the achieved measurement uncertainties we refer to the original publications.

Table 3 provides an overview of the frequencies (and their uncertainties) of the 10 measured hyperfine components belonging to the three rotational-vibrational transitions of interest. In all cases the experimental uncertainties receive appreciable contributions from statistical as well as systematic errors. In the uncertainty evaluation of the $(v, L): (0, 0) \rightarrow (0, 1)$ and $(v, L): (0, 0) \rightarrow (1, 1)$ transitions, no mention is made of possible correlated systematic errors [23, 25]. In the case of the $(v, L): (0, 3) \rightarrow (9, 3)$ transition, a correlation between two negligibly small (sub-0.01-kHz) errors in the estimate of the Zeeman shift was identified [24]. In what follows we assume the errors of all experimental transition frequencies to be uncorrelated.

$(v, L) \rightarrow (v', L')$	Label	(F, S, J)	(F', S', J')	Value (kHz)	Alt. label	Ref.
$(0, 0) \rightarrow (0, 1)$	A1	(1,2,2)	(1,2,1)	1,314,892,544.276(40)	12	[23]
	A2	(1,0,0)	(1,0,1)	1,314,916,678.487(64)	14	
	A3	(0,1,1)	(0,1,2)	1,314,923,618.028(17)	16	
	A4	(1,2,2)	(1,2,3)	1,314,935,827.695(37)	19	
	A5	(1,2,2)	(1,2,2)	1,314,937,488.614(60)	20	
	A6	(1,1,1)	(1,1,2)	1,314,937,540.762(46)	21	
$(0, 0) \rightarrow (1, 1)$	A7	(1,2,2)	(1,2,1)	58,605,013,478.03(19)	12	[25]
	A8	(1,2,2)	(1,2,3)	58,605,054,772.08(26)	16	
$(0, 3) \rightarrow (9, 3)$	A9	(0,1,4)	(0,1,4)	415,265,040,503.57(59)	$F = 0$	[24]
	A10	(1,2,5)	(1,2,5)	415,264,862,249.16(66)	$F = 1$	

Table 3. Experimentally determined transition frequencies of various hyperfine components used in the adjustment of the spin-averaged transition frequencies (Section 4). The alternate labels for the hyperfine components in column 6 are those used in the original references (column 7).

4. Global adjustment of spin-averaged transition frequencies

4.1. Adjustment details

The spin-averaged transition frequencies are determined from a global linearised least-squares adjustment of the available theoretical and experimental data presented in Secs. 2 and 3, respectively. We follow the fitting procedure described in the Appendix E of [43].

All the experimental data listed in Table 3 are included as input data for the adjustment. The associated “observational equations” (see [43] for details) read

$$\begin{aligned}
& f^{\text{exp}}[(v, L, a) \rightarrow (v', L', a')] \\
& \doteq f_{\text{SA}}[(v, L) \rightarrow (v', L')] + (E_{\text{hfs}}(v', L', a') - E_{\text{hfs}}(v, L, a)) / h \\
& + \sum_{k=1}^9 (\gamma_k(v', L', a') \delta E_k(v', L') - \gamma_k(v, L, a) \delta E_k(v, L)),
\end{aligned} \tag{4}$$

where the dotted equality sign means that the left and right hand sides are not equal in general (since the set of equations is overdetermined) but should agree within estimated errors. $a = (F, S, J)$ and $a' = (F', S', J')$ are the initial and final hyperfine states, $f_{\text{SA}}[(v, L) \rightarrow (v', L')]$ is the spin-averaged frequency of the rovibrational transition, which is to be used as a ‘pseudo-experimental’ input datum in the adjustment of fundamental constants (see Section 5). $\delta E_k(v, L)$ is an additive correction to the theoretical value of $E_k(v, L)$ that is introduced to take theoretical uncertainties into account, as done in the CODATA adjustments [1]. $\delta E_k(v, L)$ is treated as an adjusted constant, and included as an input datum with zero value and an uncertainty equal to the theoretical uncertainty of $E_k(v, L)$. However, these data are partially redundant because some pairs of coefficients are perfectly correlated to each other as explained in Section 2.1. Redundant variables are eliminated using the relationships:

$$\delta E_k(v, L) = \delta E_k(0, 0) \frac{u_k(v, L)}{u_k(0, 0)}, \quad k = 4, 5, \tag{5a}$$

$$\delta E_l(v, L) = \delta E_k(v, L) \frac{u_l(v, L)}{u_k(v, L)}, \quad (k, l) = (2, 3) \text{ or } (6, 7), \tag{5b}$$

where $u_k(v, L)$ is the uncertainty of $\delta E_k(v, L)$. There is a total of $N = 32$ input data: 10

experimental frequencies (Table 3), and 22 additive energy corrections (Table 4). The total number of adjusted constants is $M = 25$: 3 spin-averaged transition frequencies and the 22 energy corrections.

	Input datum	Value (kHz)		Input datum	Value (kHz)
B1	$\delta E_4(0, 0)$	0.000(860)	B12	$\delta E_9(1, 1)$	0.000 00(55)
B2	$\delta E_5(0, 0)$	0.000(84)	B13	$\delta E_1(0, 3)$	0.000(114)
B3	$\delta E_1(0, 1)$	0.000(116)	B14	$\delta E_2(0, 3)$	0.0000(82)
B4	$\delta E_2(0, 1)$	0.0000(83)	B15	$\delta E_6(0, 3)$	0.0000(20)
B5	$\delta E_6(0, 1)$	0.000(18)	B16	$\delta E_8(0, 3)$	0.000 000(89)
B6	$\delta E_8(0, 1)$	0.000 00(81)	B17	$\delta E_9(0, 3)$	0.000 000(60)
B7	$\delta E_9(0, 1)$	0.000 00(55)	B18	$\delta E_1(9, 3)$	0.000(62)
B8	$\delta E_1(1, 1)$	0.000(109)	B19	$\delta E_2(9, 3)$	0.0000(57)
B9	$\delta E_2(1, 1)$	0.0000(81)	B20	$\delta E_6(9, 3)$	0.0000(12)
B10	$\delta E_6(1, 1)$	0.000(17)	B21	$\delta E_8(9, 3)$	0.000 000(58)
B11	$\delta E_8(1, 1)$	0.000 00(78)	B22	$\delta E_9(9, 3)$	0.000 000(49)

Table 4. Input data for the additive energy corrections to account to the theoretical uncertainties of hyperfine interaction coefficients.

4.2. Effect of unknown hyperfine correlation coefficients

As explained in Section 2.1, the level of correlation between some of the theoretical hyperfine coefficients (namely, $E_k(v, L)$ and $E_k(v', L')$ with $k \neq 4, 5$) is not well known. We thus varied systematically their correlation coefficients between 0 and 1 to study their influence on spin-averaged frequencies. The latter were found to be mostly sensitive to the level of correlation between $E_1(v, L)$ and $E_1(v', L')$, with a smaller effect from the correlation between $E_6(v, L)$ (which itself is fully correlated with $E_7(v, L)$) and $E_6(v', L')$. Similar correlations involving other coefficients ($E_{2,3}$, E_8 , E_9) have a negligible impact. In order to estimate the additional uncertainty and possible shift caused by the unknown correlation coefficients, we carried out a Monte-Carlo simulation similar to [32], as further detailed in the Appendix A. We find that the mean shift of the simulated spin-averaged transition frequencies is well accounted for when carrying out a single adjustment using correlation coefficients of 0.5. Furthermore, we determine the full widths of the simulated frequency distributions to be 2.09 Hz, 144 Hz, and 237 Hz for the rotational, $v = 0 \rightarrow 1$, and $v = 0 \rightarrow 9$ transitions, respectively. We define a conservative measure of the frequency uncertainty associated with the unknown correlation coefficients by taking the full width divided by two. As will be shown below, these correlation-induced uncertainties are much smaller than the frequency uncertainties resulting from the adjustment itself.

In addition, the correlation-induced shifts of the three spin-averaged transition frequencies are themselves either strongly correlated or strongly anticorrelated. This implies a correlation between the adjusted spin-averaged frequencies in addition to the correlations that may result from the adjustment itself. We construct the corresponding 'correlation-induced' correlation matrix by hand from the correlation-induced uncertainties defined above, and from the observation that for variations of a single hyperfine correlation coefficient, the resulting frequency shifts to the three adjusted spin-averaged frequencies are fully (anti)correlated (see also the Appendix A).

4.3. Results and discussion

The spin-averaged frequencies determined by the least-square adjustment described above are given in the second line of Table 5.

The rotational transition is shifted by about four standard deviations with respect to the value of [23]. This is mainly due to the fact that we make different assumptions on correlations between theoretical errors, especially those between $E_4(0, 0)$ and $E_4(0, 1)$. As justified in detail in Ref. [41], we assume perfect correlation, whereas zero correlation was assumed in the initial analysis [23]. The sensitivity of the rotational transition on the assumed level of correlation was already observed in [32] (see Fig 4 (b) in that reference). For the other transitions, the frequencies determined in this work are well within the error bars of the previous determinations.

The improvement of hyperfine structure theory [41] allows reducing the uncertainties of the $v = 0 \rightarrow 1$ and $v = 0 \rightarrow 9$ transition frequencies with respect to their initial determinations [24, 25]. For the rotational transition, the precision is only slightly improved, because in this case 6 spin components have been measured, making the extracted frequency much less sensitive to theoretical uncertainties.

The normalised residuals of the adjustment (assuming a value of 0.5 for the unknown correlation coefficients) are shown in Figure 1. They reveal substantial discrepancies between the experimental data and the theoretical hyperfine structure:

- in three of the six components of the rotational transitions, labeled A1 (3.0σ or 121 Hz), A3 (2.1σ or 35 Hz), and A5 (-7.1σ or -427 Hz) (see labeling in Table 3);
- in both components of the $v = 0 \rightarrow 9$ transition, labeled A9 (-6.9σ or -4.5 kHz) and A10 (6.1σ or 3.6 kHz);
- in a few theoretical spin coefficients involved in the above two transitions, in particular $E_1(v = 0, L = 1)$ (4.2σ or 484 Hz), $E_6(v = 0, L = 1)$ (4.7σ or 85 Hz). Deviations slightly above 2σ are also found in $E_6(v = 1, L = 1)$, $E_6(v = 0, L = 3)$, $E_1(v = 9, L = 3)$, and $E_6(v = 9, L = 3)$.

Discrepancies in the hyperfine structure of these two transitions had already been evidenced and discussed in previous works [35, 41]. Their origin is presently unknown; they could be due to a problem in the theory, in the experiment, or both.

We treat these deviations following the procedure used in the CODATA adjustments (see, e.g., [1]). A multiplicative expansion factor is applied to the initially assigned uncertainties of all (experimental and theoretical) input data, such that the absolute values of all normalised residuals are smaller than two. The required expansion factor is $\eta = 3.56$. As a result, the uncertainties of the spin-averaged frequencies are multiplied by the same factor (third line in Table 5). The expanded uncertainties are one order of magnitude larger than the uncertainties associated with the unknown correlation coefficients.

The spin-averaged frequencies obtained by the least-squares adjustment have small but nonzero correlations between them due to the correlation between hyperfine theory errors δE_k in different rovibrational levels. The magnitude of the corresponding correlation coefficients is less than 0.01, and their values (and in some case also their signs) depend on the choice of hyperfine correlation coefficients (Section 2.1). Therefore, the correlations between the three adjusted spin-averaged transition frequencies have an uncertainty due to the unknown hyperfine theory correlations. In Section 5 we show that these correlations have a negligible impact on the fundamental constants that may be derived from the HD⁺ data, and we do not investigate this particular source of uncertainty further here. However, for completeness we do combine the correlation

matrix resulting from the adjustment with the correlation-induced correlation matrix that was constructed manually as described in Section 4.2. The resulting (combined) uncertainties of the spin-averaged transition frequencies are listed in the last line of Table 5, and their (combined) correlation coefficients are presented in Table 8.

	$(0, 0) \rightarrow (0, 1)$	$(0, 0) \rightarrow (1, 1)$	$(0, 3) \rightarrow (9, 3)$
f_{SA} (previous)	1 314 925 752.910(17)	58 605 052 164.24(86)	415 264 925 500.5(1.2)
$f_{\text{SA}} (\eta = 1)$	1 314 925 752.978(14)	58 605 052 164.14(16)	415 264 925 501.3(0.4)
$f_{\text{SA}} (\eta = 3.56)$	1 314 925 752.978(48)	58 605 052 164.14(55)	415 264 925 501.3(1.6)
$f_{\text{SA}} (\eta = 3.56 \text{ and corr. ind. unc.})$	1 314 925 752.978(48)	58 605 052 164.14(56)	415 264 925 501.3(1.6)

Table 5. Spin-averaged transition frequencies (in kHz). Previous determinations from the original publications [23–25] are given in the first line. The results of the least-squares adjustment performed in the present work are given in line 2. These results were obtained with an expansion factor $\eta = 1$ (i.e. no expansion factor applied). The spin-averaged frequencies in line 3 are obtained by applying an expansion factor $\eta = 3.56$ to the uncertainties of all (experimental and theoretical) input data. Finally, line 4 shows the frequencies for $\eta = 3.56$ and including the hyperfine-correlation-induced uncertainty, which are added to the uncertainty of the adjustment in quadrature. These frequencies are our recommended values.

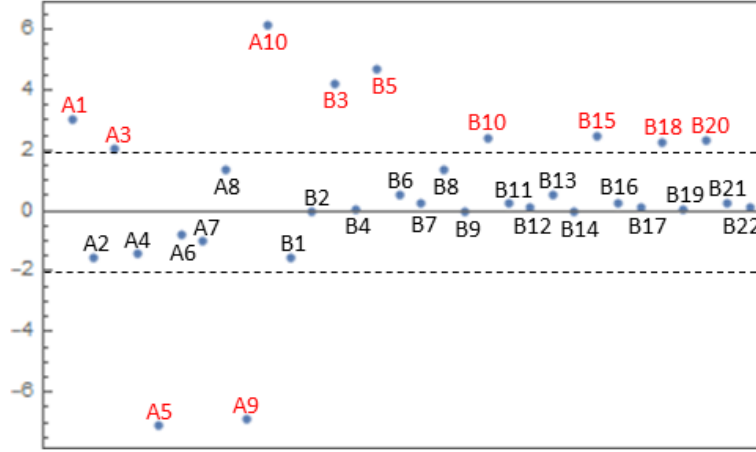


Figure 1. Normalised residuals for the adjustment of spin-averaged transition frequencies.

5. Implications for the determination of particle masses

Using the spin-averaged frequencies determined in this work, we can now assess the potential contribution of HD^+ spectroscopy to the determination of fundamental constants, in particular the relative atomic masses of the involved particles ($A_r(\text{e})$, $A_r(\text{p})$, $A_r(\text{d})$) and related mass ratios. To do this, we use a least-squares adjustment following the same procedure as in the previous section, and compare three different scenarios:

- Adjustment 1 only includes Penning trap measurements related to the electron, proton, and deuteron relative atomic masses;
- Adjustment 2 only includes HD^+ spectroscopic data and values of fundamental constants (other than atomic masses) involved in the theoretical energy levels of HD^+ ;
- Adjustment 3 includes all input data of Adjustments 1 and 2.

Theoretical rovibrational transition frequencies of HD^+ depend on the following constants [29]: the Rydberg constant (R_∞), nucleus-to-electron mass ratios ($\lambda_p \equiv m_p/m_e$

and $\lambda_d \equiv m_d/m_e$, the charge radii of the proton (r_p) and deuteron (r_d), and the fine-structure constant (α). The dependence on α is very weak because it only enters in the relativistic and QED corrections, and can be safely neglected without loss of precision. As noted in previous works, e.g., [23, 26], the mass dependence can to a good approximation be reduced to a dependence on a single parameter $\lambda_{pd} \equiv \mu_{pd}/m_e$, where μ_{pd} is the proton-deuteron reduced mass. This is exactly true in the adiabatic approximation, but, due to nonadiabatic effects, there is actually a much weaker dependence on a second mass ratio, λ_d . In our Adjustment 2, we neglect this weak dependence, allowing λ_{pd} to be determined from HD^+ spectroscopic data alone, as done in [23, 25]. Although λ_{pd} is not an adjustable parameter in Adjustment 1, it is possible to infer a value of λ_{pd} in this case from the adjusted values of $A_r(e)$, $A_r(p)$, and $A_r(d)$. The relative impact of HD^+ spectroscopy and Penning-trap measurements on future values of particle mass ratios can then be assessed by comparing the determinations of λ_{pd} (and their uncertainties) obtained from Adjustments 1 and 2. To further illustrate the effect of including HD^+ data (in addition to Penning-trap data), we also compare the values of $\lambda_p (= m_p/m_e)$ inferred from Adjustments 1 and 3.

In the perspective of a global adjustment of fundamental constants, it is preferable to take the dependence of the theoretical HD^+ transition frequencies on both parameters λ_{pd} , λ_d into account in order to avoid any unnecessary loss of precision. Furthermore, for the global Adjustment 3, we have found it more convenient to parametrise the mass dependence of HD^+ transition frequencies in terms of the quantities that are treated as adjusted parameters in the CODATA adjustments [1], i.e., the relative atomic masses $A_r(e)$, $A_r(p)$, $A_r(d)$. The linear sensitivity coefficients that describe the dependence in terms of the atomic masses are easily deduced from those describing the dependence in λ_{pd} and λ_d (see Equation (11) below).

5.1. Adjustment details

Let us briefly describe Adjustment 1. It includes the 2018 CODATA value of electron's relative atomic mass, for which no new measurement has been reported since then. For the proton relative atomic mass, we use the value of $A_r(^1\text{H})$ from the latest (2020) Atomic Mass Evaluation (AME) [44, 45], corrected for the electron mass and for the theoretical binding energy. This value takes into account recent high-precision Penning trap data [5, 6], except for a very precise measurement of the deuteron-to-proton mass ratio, m_d/m_p , performed in 2021 [7]. We thus also include the latter, together with the value of the deuteron mass deduced from the 2020 AME value of $A_r(^2\text{H})$ (again corrected for the electron mass and the binding energy), which allows improving further the proton mass determination. Adjustment 1 thus comprises $N = 4$ input data and $M = 3$ adjusted parameters, the relative atomic masses of the electron, proton and deuteron.

The other adjustments include HD^+ spectroscopic data. In Adjustment 2, each of the three spin-averaged frequencies determined in the previous section (inputs A1-A3 in Table 7) is associated with an observational equation of the form

$$\begin{aligned}
& f_{\text{SA}}[(v, L) \rightarrow (v', L')] \\
& \doteq f_{\text{SA}}^{\text{theor}}[(v, L) \rightarrow (v', L')] + \delta f(v, L, v', L') \\
& \quad + \beta_{R_\infty} c(R_\infty - R_{\infty 0}) + \eta_{r_p} (r_p^2 - r_{p0}^2) + \eta_{r_d} (r_d^2 - r_{d0}^2) \\
& \quad + \beta_{\lambda_{pd}} (\lambda_{pd} - \lambda_{pd0}) + \beta_{\lambda_d} (\lambda_d - \lambda_{d0}).
\end{aligned} \tag{6}$$

Here, $f_{\text{SA}}^{\text{theor}}[(v, L) \rightarrow (v', L')]$ is the reference value of the theoretical transition frequency [28], calculated with 2018 CODATA values of fundamental constants, and $\delta f(v, L, v', L')$ is an additive correction accounting for the theoretical uncertainty. The coefficients β , η depend on (v, L, v', L') , but for brevity this dependence is not indicated in the above equation. β_{R_∞} is the linear sensitivity coefficient to the Rydberg constant, and is simply given by

$$\beta_{R_\infty}(v, L, v', L') = \frac{f_{\text{SA}}^{\text{theor}}[(v, L) \rightarrow (v', L')]}{cR_\infty}. \quad (7)$$

In the dependence on the nuclear charge radii, following CODATA practice we only take into account the leading-order finite-size correction (see Eq. (6) of [46]). Higher-order nuclear corrections for the deuteron, which are included in the theoretical predictions [28], are taken as fixed. This yields a quadratic dependence on r_p and r_d , with coefficients η_{r_p} , η_{r_d} given by

$$\eta_{r_i}(v, L, v', L') = \eta_{r_i}(v', L') - \eta_{r_i}(v, L), \quad (8a)$$

$$\eta_{r_i}(v, L) = (2cR_\infty) \frac{2\pi}{3a_0^2} \langle \delta(\mathbf{r}_i) \rangle \quad (8b)$$

with $i = p, d$. \mathbf{r}_p (\mathbf{r}_d) is the position of the electron with respect to the proton (deuteron). Brackets denote expectation values over the nonrelativistic wavefunction of the (v, L) rovibrational state, which are calculated numerically with high precision using variational wavefunctions [27]. These expectation values are expressed in atomic units and are thus dimensionless numbers.

Finally, in order to evaluate the linear sensitivity coefficients on the mass ratios, $\beta_{\lambda_{pd}}$ and β_{λ_d} , it suffices to consider only the nonrelativistic energy levels, which yields a relative accuracy on the order of α^2 . Following the approach of [47], they can be expressed as

$$\beta_{\lambda_i}(v, L, v', L') = \beta_{\lambda_i}(v', L') - \beta_{\lambda_i}(v, L), \quad (9a)$$

$$\beta_{\lambda_{pd}}(v, L) = (2cR_\infty) \frac{1}{2} \frac{1}{\lambda_{pd}^2} \langle \nabla_{\mathbf{R}}^2 \rangle, \quad (9b)$$

$$\beta_{\lambda_d}(v, L) = (2cR_\infty) \frac{1}{\lambda_d^2} \left(\frac{1}{2} \langle \nabla_{\mathbf{r}_d}^2 \rangle + \langle \nabla_{\mathbf{R}} \cdot \nabla_{\mathbf{r}_d} \rangle \right), \quad (9c)$$

where \mathbf{R} is the position of the proton with respect to the deuteron. The expectation values are calculated numerically with high precision using variational wavefunctions [47]. They are expressed in atomic units, and are thus dimensionless numbers.

For Adjustment 3, the mass dependence is parametrised in terms of the relative atomic masses, $A_r(e)$, $A_r(p)$, and $A_r(d)$. The observational equation (6) becomes

$$\begin{aligned} & f_{\text{SA}}[(v, L) \rightarrow (v', L')] \\ & \doteq f_{\text{SA}}^{\text{theor}}[(v, L) \rightarrow (v', L')] + \delta f(v, L, v', L') \\ & \quad + \beta_{R_\infty} c(R_\infty - R_{\infty 0}) + \eta_{r_p}(r_p^2 - r_{p0}^2) + \eta_{r_d}(r_d^2 - r_{d0}^2) \\ & \quad + \beta_{A_r(e)}(A_r(e) - A_r(e)_0) + \beta_{A_r(p)}(A_r(p) - A_r(p)_0) + \beta_{A_r(d)}(A_r(d) - A_r(d)_0), \end{aligned} \quad (10)$$

where the sensitivity coefficients $\beta_{A_r(i)}$ ($i = e, p, d$) with respect to the relative atomic

Transition	$f_{\text{SA}}^{\text{theor}}$ (kHz)	β_{cR_∞}	η_{r_p} (kHz.fm ⁻²)	η_{r_d} (kHz.fm ⁻²)
(0, 0) \rightarrow (0, 1)	1 314 925 752.929	3.9969[-04]	-9.0991[-01]	-9.0991[-01]
(0, 0) \rightarrow (1, 1)	58 605 052 163.88	1.7814[-02]	-2.4253[+01]	-2.4220[+01]
(0, 3) \rightarrow (9, 3)	415 264 925 502.7	1.2623[-01]	-1.5940[+02]	-1.5850[+02]

Transition	$\beta_{\lambda_{pd}}$ (kHz)	β_{λ_d} (kHz)	$\beta_{A_r(e)}$ (kHz.u ⁻¹)	$\beta_{A_r(p)}$ (kHz.u ⁻¹)	$\beta_{A_r(d)}$ (kHz.u ⁻¹)
(0, 0) \rightarrow (0, 1)	-1.0601[+06]	-3.2126[+01]	2.3653[+12]	-8.5857[+08]	-2.1492[+08]
(0, 0) \rightarrow (1, 1)	-2.3201[+07]	-7.0874[+02]	5.1767[+13]	-1.8790[+10]	-4.7036[+09]
(0, 3) \rightarrow (9, 3)	-1.2580[+08]	-3.9569[+03]	2.6664[+14]	-9.6785[+10]	-2.4227[+10]

Table 6. Reference theoretical values and sensitivity coefficients of HD⁺ transition frequencies. The theoretical frequencies are calculated using 2018 CODATA values of $A_r(e)$, $A_r(p)$, $A_r(d)$, cR_∞ , r_p , r_d , and α . The sensitivity to the Rydberg constant β_{cR_∞} is dimensionless.

masses are given by

$$\beta_{A_r(i)}(v, L, v', L') = \frac{\partial \lambda_{pd}}{\partial A_r(i)} \beta_{\lambda_{pd}}(v, L, v', L') + \frac{\partial \lambda_d}{\partial A_r(i)} \beta_{\lambda_d}(v, L, v', L'), \quad (11)$$

where it is understood that the mass ratios are expressed in terms of the relative atomic masses: $\lambda_{pd} = A_r(p)A_r(d)/(A_r(e)[A_r(p) + A_r(d)])$, and $\lambda_d = A_r(d)/A_r(e)$. The theoretical frequencies and all the sensitivity coefficients appearing in Eqs. (6) and (10) are given in Table 6. They are calculated using reference (CODATA 2018) values of the involved fundamental constants. The dependence of the sensitivity coefficients on fundamental constants is weak, so that the values of Table 6 can be safely used during all iterations of the least-squares adjustment procedure. Note that the theoretical frequencies differ very slightly from those given in [28] because they are calculated with 2018 CODATA values of $A_r(e)$, $A_r(p)$ and $A_r(d)$, whereas the values of [28] were obtained with 2018 CODATA values of m_p/m_e and m_d/m_e . When switching between these two parametrizations, round-off errors in the published recommended values cause tiny shifts in the nonrelativistic energy levels.

Similarly to the hyperfine structure, theoretical uncertainties are accounted for by introducing additive corrections $\delta f(v, L, v', L')$ to the theoretical frequencies $f_{\text{SA}}^{\text{theor}}[(v, L) \rightarrow (v', L')]$. They are treated as adjusted constants, and included as input data with zero value and an uncertainty equal to the theoretical uncertainty of $f_{\text{SA}}^{\text{theor}}[(v, L) \rightarrow (v', L')]$. The theoretical uncertainties (B1-B3 in Table 7) and their correlation coefficients (listed in Table 8) are estimated using the results of [28]. Correlation coefficients are found to be close to 1, because the uncertainties are dominated by unevaluated QED terms, whereas numerical errors are negligibly small.

In Adjustments 2 and 3, we also include the 2018 CODATA values of the other involved fundamental constants, i.e. the Rydberg constant and the proton and deuteron radii, in order to account for their uncertainties (C5-C7 in Table 7). The fine-structure constant is not included since its uncertainty has a negligibly small influence. In total, Adjustment 2 contains $N = 9$ input data and $M = 7$ adjusted parameters: λ_{pd} , R_∞ , r_p , r_d , and the additive corrections for the three rovibrational transition frequencies.

Adjustment 3 combines the input data of the first two adjustments, with $N = 13$ input data and $M = 9$ adjusted parameters.

Label	Input datum	Value	Rel. Uncertainty	Reference
A1	$f_{\text{SA}}[(0,0) \rightarrow (0,1)]$	1 314 925 752.978(48) kHz	3.7×10^{-11}	this work
A2	$f_{\text{SA}}[(0,0) \rightarrow (1,1)]$	58 605 052 164.14(56) kHz	9.6×10^{-12}	this work
A3	$f_{\text{SA}}[(0,3) \rightarrow (9,3)]$	415 264 925 501.3(1.6) kHz	3.9×10^{-12}	this work
B1	$\delta f(0, 0, 0, 1)$	0.000(19) kHz		[28]
B2	$\delta f(0, 0, 1, 1)$	0.00(49) kHz		[28]
B3	$\delta f(0, 3, 9, 3)$	0.0(3.2) kHz		[28]
C1	$A_{\text{r}}(\text{e})$ (CODATA 2018)	$5.485\,799\,090\,65(16) \times 10^{-4}$ u	2.9×10^{-11}	[1]
C2	$A_{\text{r}}(\text{d})$ (AMDC 2020)	2.013 553 212 537(15) u	7.5×10^{-12}	[44]
C3	$A_{\text{r}}(\text{p})$ (AMDC 2020)	1.007 276 466 587(14) u	1.4×10^{-11}	[44]
C4	$m_{\text{d}}/m_{\text{p}}$ (Fink 2021)	1.999 007 501 272(9)	4.5×10^{-12}	[7]
C5	cR_{∞} (CODATA 2018)	3 289 841 960 250.8(6.4) kHz	1.9×10^{-12}	[1]
C6	r_{p} (CODATA 2018)	0.8414(19) fm	2.2×10^{-3}	[1]
C7	r_{d} (CODATA 2018)	2.12799(74) fm	3.5×10^{-4}	[1]

Table 7. Input data for the adjustments discussed in Section 5.

Correlation coefficients			
$r(\text{A1}, \text{A2}) = 0.00036$	$r(\text{A1}, \text{A3}) = 0.00644$	$r(\text{A2}, \text{A3}) = 0.00741$	$r(\text{B1}, \text{B2}) = 0.99570$
$r(\text{B1}, \text{B3}) = 0.95733$	$r(\text{B2}, \text{B3}) = 0.97998$	$r(\text{C1}, \text{C5}) = 0.00704$	$r(\text{C1}, \text{C6}) = -0.00133$
$r(\text{C1}, \text{C7}) = 0.00317$	$r(\text{C2}, \text{C3}) = 0.31986$	$r(\text{C5}, \text{C6}) = 0.88592$	$r(\text{C5}, \text{C7}) = 0.90366$
$r(\text{C6}, \text{C7}) = 0.99165$			

Table 8. Values of all nonzero correlation coefficients in the input data of Table 7.

Adjustment	Input data	Adjusted value	u_{r} (10^{-11})
1	C1-C4	$\lambda_{\text{pd}} = 1\,223.899\,228\,646(37)$	3.0
2	A,B,C5-C7	$\lambda_{\text{pd}} = 1\,223.899\,228\,719(26)$	2.1
1	C1-C4	$\lambda_{\text{p}} = 1\,836.152\,673\,353(56)$	3.0
3	All	$\lambda_{\text{p}} = 1\,836.152\,673\,423(33)$	1.8

Table 9. Adjustment results. u_{r} stands for relative uncertainty.

5.2. Results and discussion

The determinations of λ_{pd} and of the proton-electron mass ratio, λ_p , from the adjustments described above are shown in Table 9.

Adjustment 1 illustrates the potential precision permitted by Penning trap measurements alone. The relative uncertainty of λ_{pd} is found to be 3.0×10^{-11} , mainly limited by the electron’s relative atomic mass that has a relative uncertainty of 2.9×10^{-11} (see Table 7). The contribution from the proton and deuteron relative atomic masses to the uncertainty of λ_{pd} is 7.6×10^{-12} .

Adjustment 2 provides an alternative determination of λ_{pd} from HD^+ spectroscopic data. Its uncertainty is slightly smaller (2.1×10^{-11}), and the obtained values are in reasonable agreement, with a mild (1.6σ) tension. Since the precision of the first adjustment is limited by the electron’s atomic mass, the smaller uncertainty from HD^+ data indicates that the impact of HD^+ on the global CODATA adjustment would primarily be to improve the precision of $A_r(e)$.

This is verified in the last adjustment (Adjustment 3), which illustrates the potential improvement that can be obtained by combining Penning trap with HD^+ spectroscopy data. Whereas the proton and deuteron atomic masses are very precisely determined by mass spectrometry, HD^+ spectroscopy, being sensitive to the nucleus-to-electron mass ratios, provides a link to the electron mass, allowing to improve the precision of $A_r(e)$ (not shown in Table 9) and m_p/m_e to 1.8×10^{-11} , which for the latter would represent an improvement by more than a factor of three over its 2018 CODATA uncertainty. It is worth noting that the adjustment reveals no significant tension in the data, all the normalised residuals being smaller than 1.2 in absolute value.

We carried out Adjustment 3 taking into account the weak correlations between the adjusted experimental spin-averaged frequencies, discussed in Section 4.3. To assess the influence of these correlations, we repeated Adjustment 3 assuming zero correlation between the spin-averaged frequencies. The value of m_p/m_e obtained from this adjustment is identical to the one shown in the last line of Table 9, indicating a negligible impact of these correlations on the determination of fundamental constants from recent HD^+ theory and measurements.

6. Conclusion

In conclusion, we have carried out a comprehensive analysis of the available high-precision spectroscopic data of rotational and vibrational transitions in HD^+ , with the aim of providing a set of spin-averaged rotational-vibrational transition frequencies that can serve as input data for future CODATA adjustments of the fundamental physical constants. A crucial part of the analysis involves the use of theoretically computed hyperfine structure to remove hyperfine shifts from the measured transition frequencies, taking into account correlated theory errors between the various rotational-vibrational levels involved. The experimental input data are complemented by the most recent theoretical predictions of the spin-averaged transition frequencies, and by linearised expressions that parametrise these theoretical predictions in terms of relevant fundamental constants. Uncertainties and correlation coefficients pertaining to the input data were also provided, which completes the set of observational equations and covariances needed for future CODATA adjustments. To illustrate the potential of the HD^+ data, we have carried out adjustments of the electron, proton and deuteron relative atomic mass using state-of-the-art data from Penning-trap mea-

surements as well as the HD^+ data presented here, using the resulting proton-electron mass ratio as a benchmark. We thus found that the HD^+ data have a particularly large impact on the precision of the electron relative atomic mass which, together with the precise values of the proton and deuteron relative atomic masses from Penning-trap measurements, may improve the precision of m_p/m_e by more than a factor of three compared to the current 2018 CODATA value.

Acknowledgement(s)

The authors warmly thank Wim Ubachs for his invaluable contributions and continued support to the Amsterdam-Paris HD^+ research collaboration.

Disclosure statement

The authors report there are no competing interests to declare.

References

- [1] E. Tiesinga, P.J. Mohr, D.B. Newell and B.N. Taylor, *Rev. Mod. Phys.* **93**, 025010 (2021).
- [2] S. Sturm, F. Köhler, J. Zatorski, A. Wagner, Z. Harman, G. Werth, W. Quint, C.H. Keitel and K. Blaum, *Nature* **506**, 467–470 (2014).
- [3] F. Heiße, F. Köhler-Langes, S. Rau, J. Hou, S. Junck, A. Kracke, A. Mooser, W. Quint, S. Ulmer, G. Werth, K. Blaum and S. Sturm, *Phys. Rev. Lett.* **119** (3), 033001 (2017).
- [4] F. Heiße, S. Rau, F. Köhler-Langes, W. Quint, G. Werth, S. Sturm and K. Blaum, *Phys. Rev. A* **100**, 022518 (2019).
- [5] S. Rau, F. Heiße, S. Köhler-Langes, F. Sasidharan, R. Haas, D. Renisch, C.E. Düllmann, W. Quint, S. Sturm and K. Blaum, *Nature* **585**, 43–47 (2020).
- [6] D.J. Fink and E.G. Myers, *Phys. Rev. Lett.* **124**, 013001 (2020).
- [7] D.J. Fink and E.G. Myers, *Phys. Rev. Lett.* **127**, 243001 (2021).
- [8] W.H. Wing, G.A. Ruff, W.E. Lamb and J.J. Spezeski, *Phys. Rev. Lett.* **36**, 1488–1491 (1976).
- [9] M. Hori, A. Dax, J. Eades, K. Gomikawa, R.S. Hayano, N. Ono, W. Pirkel, E. Widmann, H.A. Torii, B. Juhász, D. Barna and D. Horváth, *Phys. Rev. Lett.* **96**, 243401 (2006).
- [10] M. Hori, A. Sótér, D. Barna, A. Dax, R. Hayano, S. Friedreich, B. Juhász, T. Pask, E. Widmann, D. Horváth, L. Venturelli and N. Zurlo, *Nature* **475**, 484–488 (2011).
- [11] M. Hori, H. Aghai-Khozani, A. Sótér, D. Barna, A. Dax, R. Hayano, T. Kobayashi, Y. Murakami, K. Todoroki, H. Yamada, D. Horváth and L. Venturelli, *Science* **354**, 610–614 (2016).
- [12] P.J. Mohr, B.N. Taylor and D.B. Newell, *Rev. Mod. Phys.* **80**, 633–730 (2008).
- [13] P.J. Mohr, B.N. Taylor and D.B. Newell, *Rev. Mod. Phys.* **84**, 1527–1605 (2012).
- [14] P. Blythe, B. Roth, U. Fröhlich, H. Wenz and S. Schiller, *Phys. Rev. Lett.* **95**, 183002 (2005).
- [15] B. Roth, J.C.J. Koelemeij, H. Daerr and S. Schiller, *Phys. Rev. A* **74** (4), 040501(R) (2006).
- [16] J.C.J. Koelemeij, B. Roth, A. Wicht, I. Ernsting and S. Schiller, *Phys. Rev. Lett.* **98** (17), 173002 (2007).
- [17] J.C.J. Koelemeij, D.W.E. Noom, D. de Jong, M.A. Haddad and W. Ubachs, *Appl. Phys. B-Lasers Opt.* **107** (4), 1075–1085 (2012).
- [18] J. Schmidt, T. Louvradoux, J. Heinrich, N. Sillitoe, M. Simpson, J.P. Karr and L. Hilico, *Phys. Rev. Applied* **14**, 024053 (2020).

- [19] U. Bressel, A. Borodin, J. Shen, M. Hansen, I. Ernsting and S. Schiller, Phys. Rev. Lett. **108** (18), 183003 (2012).
- [20] S. Alighanbari, M.G. Hansen, V.I. Korobov and S. Schiller, Nat. Phys. **14** (6), 555–559 (2018).
- [21] J. Biesheuvel, J.-Ph. Karr, L. Hilico, K.S.E. Eikema, W. Ubachs and J.C.J. Koelemeij, Nat. Commun. **7**, 10385 (2016).
- [22] J. Biesheuvel, J.-Ph. Karr, L. Hilico, K.S.E. Eikema, W. Ubachs and J.C.J. Koelemeij, Appl. Phys. B-Lasers Opt. **123** (1), 23 (2017).
- [23] S. Alighanbari, G.S. Giri, F.L. Constantin, V.I. Korobov and S. Schiller, Nature **581**, 152–158 (2020).
- [24] S. Patra, M. Germann, J.-Ph. Karr, M. Haidar, L. Hilico, V.I. Korobov, F.M.J. Cozijn, K.S.E. Eikema, W. Ubachs and J.C.J. Koelemeij, Science **369** (6508), 1238–1241 (2020).
- [25] I.V. Kortunov, S. Alighanbari, M.G. Hansen, G.S. Giri, V.I. Korobov and S. Schiller, Nat. Phys. **17**, 569–573 (2021).
- [26] V.I. Korobov, L. Hilico and J.-Ph. Karr, Phys. Rev. Lett. **118**, 233001 (2017).
- [27] D.T. Aznabayevev, A.K. Bekbaev and V.I. Korobov, Phys. Rev. A **99**, 012501 (2019).
- [28] V.I. Korobov and J.-Ph. Karr, Phys. Rev. A **104**, 032806 (2021).
- [29] J.-Ph. Karr, L. Hilico, J.C.J. Koelemeij and V.I. Korobov, Phys. Rev. A **94**, 050501(R) (2016).
- [30] S.G. Karshenboim and V.G. Ivanov, Applied Physics B: Lasers and Optics **123** (1), 18 (2017).
- [31] A. Antognini, S. Bacca, A. Fleischmann, L. Gastaldo, F. Hagelstein, P. Indelicato, A. Knecht, V. Lensky, B. Ohayon, V. Pascalutsa, N. Paul, R. Pohl and F. Wauters, Muonic-Atom Spectroscopy and Impact on Nuclear Structure and Precision QED Theory. arXiv:2210.16929 [nucl-th] arXiv 2022. <<https://arxiv.org/abs/2210.16929>>.
- [32] J.C.J. Koelemeij, Molecular Physics **120** (19-20), e2058637 (2022).
- [33] D. Bakalov, V.I. Korobov and S. Schiller, Phys. Rev. Lett. **97**, 243001 (2006).
- [34] V.I. Korobov, Phys. Part. Nucl. **53**, 787 (2022).
- [35] J.-Ph. Karr, M. Haidar, L. Hilico, Z.X. Zhong and V.I. Korobov, Phys. Rev. A **102**, 052827 (2020).
- [36] A. Layzer, Nuovo Cim. **33**, 1538 (1964).
- [37] D.E. Zwanziger, Nuovo Cim. **34**, 77 (1964).
- [38] G.T. Bodwin and D.R. Yennie, Phys. Rev. D **37**, 498 (1988).
- [39] V.I. Korobov, J.P. Karr, M. Haidar and Z.X. Zhong, Phys. Rev. A **102**, 022804 (2020).
- [40] M. Haidar, V.I. Korobov, L. Hilico and J.P. Karr, Phys. Rev. A **106**, 022816 (2022).
- [41] M. Haidar, V.I. Korobov, L. Hilico and J.P. Karr, Phys. Rev. A **106**, 042815 (2022).
- [42] M. Puchalski, J. Komasa and K. Pachucki, Phys. Rev. Lett. **125** (2020).
- [43] P.J. Mohr and B.N. Taylor, Rev. Mod. Phys. **72**, 351–495 (2000).
- [44] M. Wang, W.J. Huang, F.G. Kondev, G. Audi and S. Naimi, Chin. Phys. C **45** (3), 030003 (2021).
- [45] W.J. Huang, M. Wang, F.G. Kondev, G. Audi and S. Naimi, Chin. Phys. C **45** (3), 030002 (2021).
- [46] V.I. Korobov, Phys. Rev. A **74**, 052506 (2006).
- [47] S. Schiller and V. Korobov, Phys. Rev. A **71**, 032505 (2005).

Appendix A. Monte-Carlo simulation

To assess the uncertainty associated with the unknown correlation coefficients $r[E_k(v, L), E_k(v', L')] \equiv r_k$ (with $k \neq 4, 5$) we carry out a Monte-Carlo simulation analogous to [32]. As explained in Section 4.1, we set $r_2 = r_3$ and $r_6 = r_7$. We subsequently choose random values from the interval $[0, 1)$ for each of the coefficients of the vector $(r_1, r_2, r_6, r_8, r_9)$, and carry out the adjustment of the spin-averaged frequencies

and the terms $\delta E_k(v, L)$. This is repeated 500 times, and in addition for the vectors $(0, 0, 0, 0, 0)$ and $(1 - \epsilon, 1 - \epsilon, 1 - \epsilon, 1 - \epsilon, 1 - \epsilon)$, with $\epsilon = 10^{-6}$ to avoid singular covariance matrices. Adjustments are carried out numerically using 100 digits of precision. Histograms of the Monte-Carlo distributions of adjusted transition frequencies are shown in Figure A1. The full widths of the frequency distributions are 2.09 Hz, 144 Hz, and 237 Hz for the (v, L) : $(0, 0) \rightarrow (0, 1)$, (v, L) : $(0, 0) \rightarrow (1, 1)$ and (v, L) : $(0, 3) \rightarrow (9, 3)$ transitions, respectively; the deviation of the mean spin-averaged frequency from the frequency obtained for the $(0.5, 0.5, 0.5, 0.5, 0.5)$ case is 0.05 Hz, -3 Hz, and -2 Hz (i.e. less than 3% of the full width). Figure A1 furthermore shows the dependence of the correlation-induced shift if all correlation coefficients are varied simultaneously. Comparing the shifts of the three transitions shows that the shift of the rotational transition is anticorrelated with the shift of the $v = 0 \rightarrow 1$ and $v = 0 \rightarrow 9$ transitions, whereas the shifts for the latter two are correlated.

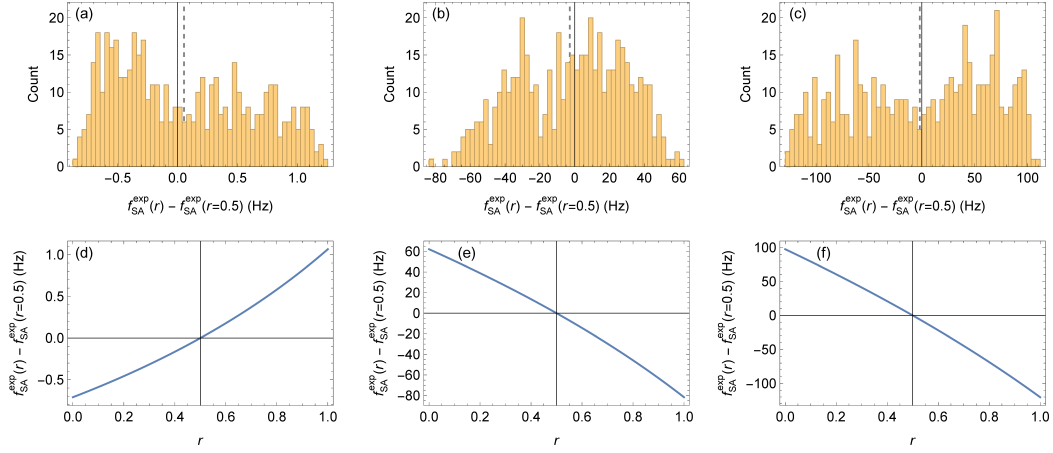


Figure A1. Distribution of correlation-induced shifts of spin-averaged frequencies obtained from a Monte-Carlo simulation consisting of 502 runs. Here the argument r represents the vector $(r_1, r_2, r_6, r_8, r_9)$; likewise $r = 0.5$ stands for the vector $(0.5, 0.5, 0.5, 0.5, 0.5)$ (a) Distribution for the $(v, L): (0,0) \rightarrow (0,1)$ transition. (b) Distribution for the $(v, L): (0,0) \rightarrow (1,1)$ transition. (c) Distribution for the $(v, L): (0,3) \rightarrow (9,3)$ transition. Dashed vertical lines indicate the mean value of the frequency distribution. (d) Frequency shift of the $(v, L): (0,0) \rightarrow (0,1)$ transition if all components of the vector r are varied simultaneously. (e) Same as (d), but for the $(v, L): (0,0) \rightarrow (1,1)$ transition. (f) Same as (d), but for the $(v, L): (0,3) \rightarrow (9,3)$ transition.